Strengths and Weaknesses of the Analytical Techniques Used for Measuring Low Mercury Mass Fractions (< 10 ng g^{-1}) in Crystalline Rocks: Direct Mercury Analyser *Versus* Cold Vapour-Atomic Fluorescence Spectroscopy

Francesco **Narduzzi** (1, 2)* ID, Stefano **Covelli** (2), Federico **Floreani** (2), Elena **Pavoni** (2), Elisa **Petranich** (2), Sarah C. **Jantzi** (3), Mattia **Pistone** (4), Ana **Černok** (2), Marco **Venier** (5), Matteo **Crosera** (6) and Luca **Ziberna** (2)

(1) Dipartimento di Scienze della Terra e dell'Ambiente, Università di Pavia, Via Ferrata 1, 2700 Pavia, Italy

(2) Dipartimento di Matematica, Informatica e Geoscienze, Università di Trieste, Via Weiss 2, 34128 Trieste, Italy

(3) Plasma Chemistry Laboratory, Center for Applied Isotope Studies, 120 Riverbend Rd, Athens, GA 30602, USA

(4) Department of Geology, University of Georgia, Franklin College of Arts and Sciences, Geography-Geology Building, 210 Field Street, Athens, GA 30602-2501, USA

(5) Institute for Geosciences, Johannes Gutenberg University of Mainz, J.-J.-Becher-Weg 21, D-55128 Mainz, Germany

(6) Dipartimento di Scienze Chimiche e Farmaceutiche, Università di Trieste, Via Licio Giorgieri 1, 34127 Trieste, Italy

* Corresponding author. e-mail: narduzzi13@gmail.com

Elemental mercury (Hg) is routinely determined in crystalline rocks with mass fractions lower than 10 ng g^{-1} by thermal decomposition using Direct Mercury Analyzer (DMA-80) or Lumex RA-915+ (equipped with a PYRO-915+ attachment) instruments, both based on atomic absorption spectroscopy. However, 223 analyses over the course of one year with DMA-80 and cold vapour-atomic fluorescence spectroscopy (CV-AFS) on three reference materials (RMs) and six crystalline rocks (granite, diorite, gabbro, spinel peridotite, phlogopite-rich peridotite, and sulfide-rich orthogneiss) from the exposed transcrustal section of the Ivrea-Verbano Zone and upper crustal Serie dei Laghi unit (western Alps, Italy) reveal that rock analyses using the DMA-80 are variably affected by different internal and external biases when Hg mass fractions are below 10 ng g^{-1}. Conversely, CV-AFS analyses are more precise, providing homogenous and repeatable results, even at ultra-low Hg mass fractions (< 1 pg g^{-1}). Furthermore, CV-AFS analyses show that gabbro and spinel peridotite powders roasted for *analysis by DMA-80* still contain ~ 0.6 to ~ 1.4 ng g^{-1} of Hg, implying inefficient release of Hg from basic/ultrabasic lithologies. Therefore, we recommend the use of CV-AFS for Hg measurements in crystalline rocks. We also propose a new Hg reference value of 3.9 $\pm$ 1.5 ng g^{-1} for the GSJ granodiorite reference material JG-1a.

Keywords: mercury, direct mercury analyzer, cold vapour-atomic fluorescence spectroscopy, reference materials, JG-1a.

Mercury (Hg) is the most volatile and among the three most toxic heavy metals (Covelli *et al.* 2001, Canil *et al.* 2015, Marie *et al.* 2014, Gworek *et al.* 2020, Torres-Rodriguez *et al.* 2024). Besides industrial and mining activities (Covelli *et al.* 2001, Gworek *et al.* 2020) and natural re-emission from land and water surfaces (Pirrone *et al.* 2010, Floreani *et al.* 2019), degassing from active volcanoes is the other remaining source capable of emitting substantial amounts of Hg into the atmosphere (Bagnato *et al.* 2014, Coufalik *et al.* 2018, Edwards *et al.* 2021, Edmonds *et al.* 2022, Kushner *et al.* 2023). However, the source and mobility of Hg in magmas before degassing remain poorly constrained (e.g., Canil *et al.* 2015) mainly due to the analytical challenges related to its chemical behaviour (Marie *et al.* 2014) and low abundance in crystalline rocks (mostly < 40 ng g^{-1}, Figure 1).

To date, a literature search of 767 Hg determinations in rocks showed that 46% were carried out with a DMA-80

Direct Mercury Analyser, 30% with a Lumex RA-915+ instrument equipped with a PYRO-915+ attachment (hereafter Lumex RA-915+), 14% with other techniques (atomic fluorescence, acid digestion with atomic absorption spectroscopy or AAS, 1:1:1 *aqua regia* digestion with ultra-trace inductively coupled plasma-mass spectrometry or ICP-MS; cold vapour multicollector (MC-) ICP-MS and neutron activation analyses not considered in this work), 8% with Cold Vapour-Atomic Fluorescence Spectroscopy (CV-AFS), and the remaining < 2% with Advanced Mercury Analyzer

(AMA-254) (Figure 1; Marowsky and Wedepohl 1971, Coderre and Steinthórsson 1977, Garuti *et al.* 1984, Gao *et al.* 1998, Pitcairn *et al.* 2006b, 2010, 2015, Zintwana *et al.* 2012, Canil *et al.* 2015, Coufalik *et al.* 2015, Hammerli *et al.* 2016, Smith *et al.* 2008, Wang *et al.* 2021, Deng *et al.* 2022a, b, Yin *et al.* 2022, Tian *et al.* 2023). Therefore, DMA-80 and Lumex RA-915+ are the most used instruments to measure Hg in crystalline rocks due to their capability for fast, direct measurement of Hg through the combustion of a solid sample (i.e., powder), limiting
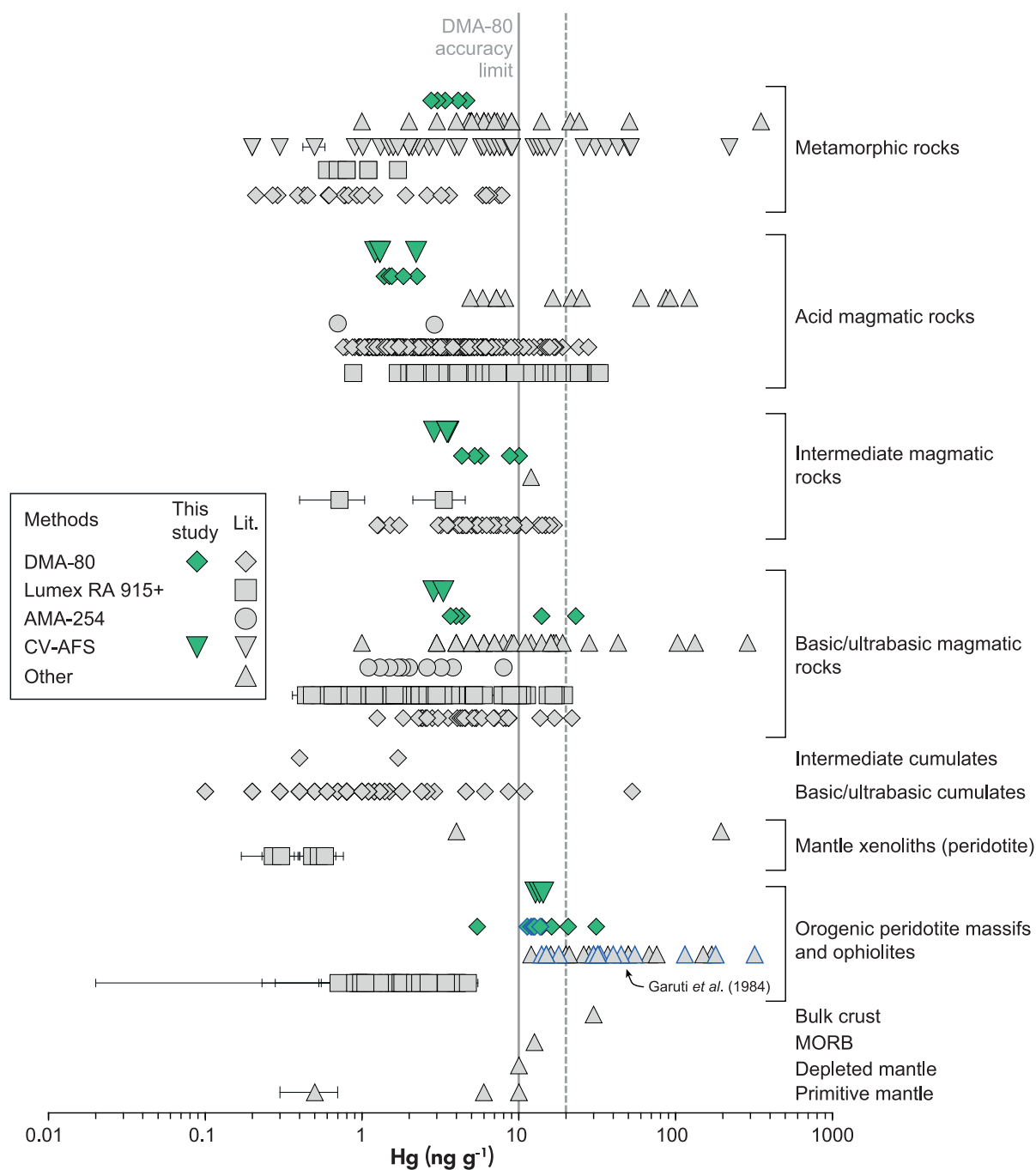
Figure 1. Mercury mass fraction (ng g^{-1}) for different magmatic and metamorphic rocks (n = 767) measured by several analytical methods (see online supporting information Table S1) and compared with the results of this study. We did not plot the mass fraction of sedimentary protoliths analysed by Pitcairn *et al.* (2006b, 2010), and we considered only the results we judged uncontaminated (unless specified, i.e., Garuti *et al.* 1984). Each point represents a single analysis or the mean of two to five replicates for the same sample. All error bars associated with data points represent 2*s*, also for the literature values for which the standard deviations were unreported, or reported as 1*s*. Some 2*s* values are smaller than the symbols, while others are larger than the absolute value and, in the latter case, are not shown. Some of the CV-AFS data are the mean of two to twenty samples. Grey solid and dotted lines indicate the 10 and 20 ng g^{-1} accuracy limits, respectively of the DMA-80 after Marie *et al.* (2014). Mercury mass fractions for the Balmuccia peridotite samples by DMA-80 (this study) and by Garuti *et al.* (1984) are shown with blue rims. See text for more information. Data are from Marowsky and Wedepohl (1971), Coderre and Steinthórsson (1977), Garuti *et al.* (1984), Gao *et al.* (1998), Pitcairn *et al.* (2006b, 2010, 2015), Zintwana *et al.* (2012), Canil *et al.* (2015), Coufalik *et al.* (2015), Hammerli *et al.* (2016), Smith *et al.* (2008), Wang *et al.* (2021), Deng *et al.* (2022a, b), Yin *et al.* (2022) and Tian *et al.* (2023). Bulk crust (Rudnick and Gao (2014), depleted mantle (Salters and Strake 2004), MORB (Arevalo and McDonough 2010), and primitive mantle (McDonough and Sun 1995, Palme and O'Neil 2014, Canil *et al.* 2015) are plotted for comparison.

additional sample manipulation (e.g., acid digestion) and potential contamination (Marie *et al.* 2014). From the agreement between the mass fraction measurements on different reference materials (RMs) and their certified values and within-batch analyses (i.e., replicates), Marie *et al.* (2014) proposed that the DMA-80 has good accuracy and precision for Hg mass fractions from 10 to 6000 ng g^{-1}. The same authors also indicate that Hg determination on different RMs, when compared with recommended values in literature, had the best fit (i.e., increase in the correlation coefficient R^2) above 20 ng g^{-1}. However, of the 46% of the literature Hg measurements done by DMA-80, 91% of the rocks have mass fractions ≤ 10 ng g^{-1} and 99% ≤ 20 ng g^{-1} (Figure 1). In other words, so far, this instrument has been used to measure Hg in rocks with mass fractions that are often below its accuracy limit (10 ng g^{-1}), as defined by Marie *et al.* (2014).

Further uncertainty about the reliability of DMA-80 results might be related to its combustion efficiency. DMA-80 heats the powder to 650 °C for 1 min at 1 atm to release Hg from the compound (Marie *et al.* 2014). Nonetheless, most rocks have solidus temperatures ($T_{solidus}$) higher than 650 °C at 1 atm (e.g., Stern *et al.* 1975, Ulmer 2000). This raises doubts on the possibility that all Hg can be released from sample powders during only one minute of combustion without melting.

Considering other mechanisms of Hg mobility that could trigger Hg loss, diffusion cannot be the mechanism that triggers the release of all the Hg, assuming it is partitioned into the crystal lattices of the rock-forming minerals (e.g., Jovanovic

and Reed, 1968), because of the short duration of the combustion (1 min). Further rarely considered complexities that can lead to uncertainties in determining Hg are its volatilisation during sample powdering, sample heterogeneity (i.e., nugget effect), the quantity of powder used for the analyses, and powder grain sizes (e.g., Mendelez-Perez and Fostier, 2013, Marie *et al.* 2014, Canil *et al.* 2015).

The Lumex RA-915+ and AMA-254 analytical methods are not so different from the DMA-80 and have detection limits of 0.5 and 3 ng g^{-1}, respectively (Sholupov *et al.* 2004, Coufalik *et al.* 2015). However, because the Lumex RA-915+ lacks the Au-amalgamator present in DMA-80 and AMA 254, its accuracy and precision should be very limited at lower Hg mass fractions. In addition, Lumex RA-915+ and AMA 254 have never been adequately tested for their efficiency in measuring Hg in crystalline rocks. Hence, the doubts outlined for the DMA-80 are also valid for Lumex RA-915+ because of the 30% of all analyses carried out with this technique (Figure 1), 74% are ≤ 10 ng g^{-1} and 91% are ≤ 20 ng g^{-1}, while for the AMA-254 analyses are entirely ≤ 8 ng g^{-1}.

The CV-AFS technique is far less frequently used for measuring Hg in crystalline rock, as indicated by the 8% of the analyses in Figure 1. This is because it is time-consuming and may suffer from contamination during sample preparation. Nonetheless, by applying attentive protocols that mitigate or prevent contamination, this analytical method is potentially more accurate and precise and has a very low detection limit (1 pg g^{-1}), as demonstrated in different studies (Bloom and Fitzgerald 1988, Hageman 2007, Pitcairn

et al. 2006a, 2010, 2015, Butcher 2019). The only documented scientific works applying this methodology for crystalline rocks can be found in Pitcairn et al. (2006a, 2010, 2015), who measured Hg mass fractions from ~ 70 down to 1 ng g^{-1} in unmetamorphosed to amphibolite facies sedimentary and basaltic rocks of the Otago and Alpine Schists, New Zealand.

This work aims to report DMA-80 and CV-AFS analyses on different RMs and crystalline rock samples to test the accuracy and precision of DMA-80 in measuring Hg mass fractions below 10 ng g^{-1}. In doing so, we also consider potential biases that could affect the measurements, such as Hg volatilisation during sample preparation, contamination, nugget effect, the amount of powder used for the analyses, and powder grain sizes. Lastly, we compare our results with those published so far to provide a new perspective on the reliability of the published data, as well as propose a new reference value for the GSJ JG-1a granodiorite (Geological Survey of Japan) RM.

Geological settings and materials

The six samples used in this work are from the Ivrea-Verbano Zone and adjacent Serie dei Laghi unit (IVZ and SdL, respectively; northwest Italy, Figure 2). The IVZ and SdL represent an almost complete section of the continental crust tiled by ~ 90° during Alpine orogenesis and hosting a quasi-continuous transcrustal igneous section (i.e., the Sesia Magmatic System) traceable from its deepest roots to the exposed caldera (e.g., Sinigoi et al. 2016, Karakas et al. 2019, Pistone et al. 2020, Tavazzani et al. 2023). The IVZ exposes a ~ 10 km thick lower crustal Permian Mafic Complex, consisting mainly of gabbroic and dioritic rocks, intruding into the Kinzigite Formation, which is a Palaeozoic volcano-sedimentary sequence metamorphosed in amphibolite to granulite facies. The SdL consists of upper crustal low amphibolite-facies schists and gneisses intruded by the Permian granitic bodies composing the Graniti dei Laghi. The SdL and Graniti dei Laghi are overlaid by coeval rhyolitic caldera-fill deposits (i.e., Sesia Caldera). The optical petrographic screening of the six samples led to the following observations.

Sample LS149 is a homogeneous monzogranite from the upper crustal Valle Mosso pluton of the SdL (Figure 2; Tavazzani et al. 2017, 2020). It is medium to coarse-grained with a hypidiomorphic texture. Major minerals are quartz, K-feldspar, plagioclase and chloritised biotite. Accessory minerals are muscovite, epidote, zircon, apatite and rare sulfides (< 0.1% by volume).

Sample VS134 is a diorite of the Mafic Complex (Figure 2; Sinigoi et al. 2016). It is hypidiomorphic and medium- to coarse-grained. Plagioclase, orthopyroxene, clinopyroxene, amphibole, and biotite are the main rock-forming minerals. The accessory minerals include sulfides (~ 2 vol.%), Fe-oxides, zircons, and apatites.

Sample Campore dyke is a ~ 10- to 15 m-wide mafic intrusion at the base of the Valle Mosso pluton (Figure 2) and is classified as gabbro (Tavazzani et al. 2017, Sinigoi et al. 2016). The sample collected from the central part of the intrusion shows an ophitic texture with medium to coarse-grained plagioclase and amphibole. Accessory minerals are zircon, apatites, Fe-oxides, and sulfides (~ 2 vol.%), sometimes up to 1 cm.

Sample NZ2314A2 is from the Balmuccia peridotite body and was collected from a disused quarry on the north of the Sesia River (Figure 2). It is a foliated lherzolite with a porphyroclastic recrystallised texture. Olivine, orthopyroxene, and clinopyroxene are the main rock-forming minerals. Sulfides (~ 5 vol.%) and spinels are accessory minerals.

Sample F9 peridotite is from the Finero peridotitic body (Figure 2), dominantly showing protogranular, although locally displaying porphyroclastic recrystallised texture. Olivine, orthopyroxene, and phlogopite are abundant, while clinopyroxene and amphibole are less common. Accessory
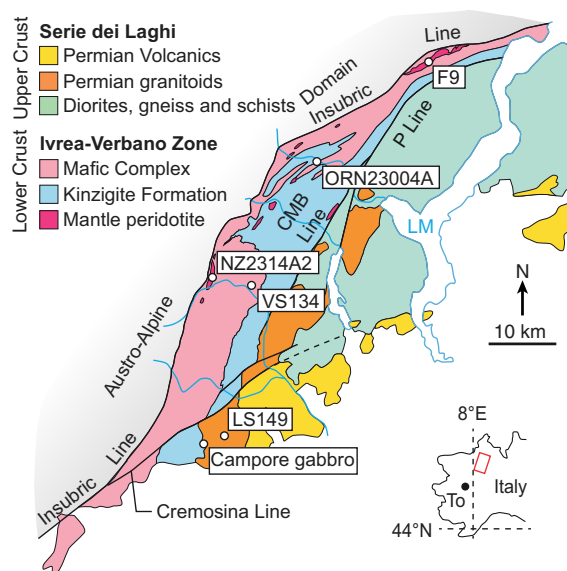

Figure 2. Geological map of Ivrea-Verbano Zone and Serie dei Laghi unit (after Tavazzani et al. 2020) with the of sample locations indicated. P Line: Pogallo Line; CMB Line: Cossato–Mergozzo–Brissago Line.

minerals are rare sulfides (< 0.1 vol.%), spinels, apatites and zircons.

Sample ORN23004A is a medium- to fine-grained banded orthogneiss sampled near the old mines of Migiandone near Ornavasso (Figure 2). The sample consists of biotite, amphibole, garnet, pyroxene, and plagioclase as major minerals. Sulfides are up to ~ 2 vol.% and are minor minerals, while oxides, titanites, apatite, and zircons are all accessory minerals.

Materials and methods

Sample preparation

Before grinding and powdering the samples, their petrographic properties were inspected by focusing the screening on detecting any internal weathering that could bias the Hg results. Selected unaltered samples were cut with a water-cooled diamond saw into ~ 0.5 cm-thick slices and rapidly dried with compressed air to mitigate chemical weathering via oxidative leaching of sulfides (Peters 1976). Rock slices were cleaned from saw marks, blade paint, pen marks, and minor weathered surfaces with a water-cooled diamond polishing pad, washed in water, and rapidly dried with compressed air. Cleaned slices were crushed into small chips (< 5 mm) using a hammer and anvil. To limit potential contamination between samples and surfaces used to grind the samples, it is common practice to use plastic trays and/or clean paper sheets to minimise contact (e.g., Pitcairn et al. 2006b, Wang et al. 2013). This procedure was not adopted since Hg might be present in variable quantities in plastic and paper, and microscopic pieces of both materials could unintentionally become part of the sample during grinding, leading to possible spurious results. Hence, hammer and anvil surfaces were pre-conditioned for each sample by grinding a small amount of the sample targeted for the Hg determinations to a fine powder. The ground material was then discarded, and only that from the second hammering was collected. Hammer and anvil surfaces were cleaned before and after each pre-conditioning and grinding step with abundant acetone, high-purity (Milli-Q) water, and compressed air. No other treatment, such as drying or sieving, was applied.

For each sample, we collected between 200 and 300 g of material, which was split into four batches and subsequently subjected to different pulverisation treatments. Depending on the pulverisation method used and to include all mineral phases, we powdered between 10 and 60 g for

each batch. The first batch was powdered by hand with agate mortar and pestle (AM); the second was powdered by agate ball mill pulverisette (AP); and the third was powdered by tungsten carbide pulverisette (WCP) (Table 1). The fourth batch was passed through a jaw crusher before powdering with AP (JAP). The same pre-conditioning method was also applied to the rock pulverisation step that helps prevent any bias due to possible contamination. In addition, we aimed to produce monodisperse sample powders displaying grain sizes as homogeneous as possible. Heterogeneous grain sizes (polydisperse suspension) might lead to incomplete Hg release during combustion at the DMA-80 or incomplete grain dissolution during the acid digestion step before CV-AFS analyses (see below). To overcome this problem, the time of powdering for each sample was set at 1 h for the AP and JAP (30 min with 30 mm agate spheres and 30 min with mixed 10 to 15 mm agate spheres), 30 min for the AM, and 2 min for the WCP. The low powdering time for the WCP was set to prevent any instrumental damage. A small aliquot of each powder was inspected under a Leica stereographic microscope to investigate the grain sizes. Online supplementary materials show an example from Campore gabbro and NZ2314A2 Balmuccia peridotite powders (Figures S1 and S2, respectively). Hand-made powders (AM) show heterogeneous grain sizes, with most grains larger than 100 μm. Conversely, AP powders are homogeneous and show grain sizes well below 100 μm.

It has been suggested that during long planetary milling sessions, the increase in temperature inside the agate and tungsten carbide jars heats the powder and can cause Hg losses through volatilisation (e.g., Canil et al. 2015). To investigate this possibility, we measured the temperature with a Parkside® Digital Laser Infrared Thermometer, having a temperature range between 50 to + 380 °C and a reading error for measures of ± 1.5 °C and ± 3 °C at > 0 °C and < 0 °C, respectively. Temperatures were measured less than one minute after the milling stopped by pointing the laser against the agate and tungsten carbide jar walls, agate spheres, tungsten carbide rings, and powders. All temperatures were ≤ 40 °C, even after 1 hour of powdering.

Direct Mercury Analyzer (DMA-80)

Samples were analysed for total Hg mass fraction with a Milestone double-cell model DMA-80 Direct Mercury Analyzer at the Department of Mathematics, Informatics and Geoscience of the University of Trieste (Italy). Operating conditions were similar to those described in Marie et al. (2014). Between 0.250 and 0.256 g of powder from

GEOSTANDARDS and GEOANALYTICAL RESEARCH

Table 1.
Summary of the samples, powdering methods and duration, and analytical techniques adopted in this work

Sample	Powdering method[a]	Powdering duration	Analytical method		
			DMA-80[b]	CV-AFS[c]	CV-AFS after DMA-80[d]
LS149 (Granite)	AM	30 min	x		
	WCP				
	AP	1 h	x	x	x
	JAP	1 h	x		
VS134 (Diorite)	AM	30 min	x		
	WCP	2 min	x		
	AP	1 h	x	x	
	JAP	1 h	x		
Campore dyke (Gabbro)	AM	30 min	x		
	WCP	2 min	x		
	AP	1 h	x	x	x
	JAP	1 h	x		
NZ2314A2 (Spinel-peridotite)	AM	30 min	x		
	WCP	2 min	x		
	AP	1 h	x	x	x
	JAP	1 h	x		
F9 (Phlogopite-rich peridotite)	AM	30 min	x		
	WCP	2 min	x		
	AP	1 h	x		
	JAP	1 h	x		
ORN23004A (Sulfide-rich orthogneiss)	AM	30 min	x		
	WCP	2 min	x		
	AP	1 h	x		
	JAP	1 h	x		

[a] AM: agate mortar and pestle (hand-made powders); WCP: tungsten carbide pulveristette; AP: Agate ball mill pulverisette; JAP: jaw crusher before AP.
[b] DMA-80: Direct Mercury Analyser.
[c] CV-AFS: Cold vapour-atomic fluorescence spectroscopy.
[d] Performed on roasted powder. See text for more information.

each powdered batch was weighed in nickel (Ni) coated sample boats, placed into the autosampler, and brought into the furnace for drying at 200 °C for 1 min to prevent sample loss by splashing. Samples were then heated at 650 °C for 1.5 minutes to release all Hg species as elemental Hg (Hg^0). Elemental Hg is carried to the Au trap to form amalgam by ultrapure oxygen (O$_2$ 99.9999%) used as gas carrier and for the combustion of samples. Halogens and nitrogen-sulfur oxides released during combustion are trapped in the catalyst during transport to the amalgamator while remaining gasses are purged out of the system for 1 min before Hg^0 is quantitatively desorbed by heating the Au amalgamator at 850 °C for 30 s. Elemental Hg was then measured by passing through to an atomic absorbance spectrophotometer (wavelength 253.65 nm) consisting of two sequential cells designed for low (0–20 ng) and high (20–1000 ng) Hg contents and UV-enhanced photodiodes for detection. Concentrations were calculated based on the masses of the analysed powder and detector response based on the calibration curve (EPA method 7473, USEPA 2007). It is fundamental to recall that DMA-80 performs only one measurement for each aliquot, meaning

that it cannot provide any information on within-aliquot heterogeneity and measurement repeatability. Within-sample heterogeneity was determined by analysing between three and seven aliquots for each rock sample.

Instrumental calibration was performed once using standard solutions (from 10 μg l^{-1} to 10 mg l^{-1}) prepared by diluting a Hg standard solution (Merck Millipore, 1000 mg l^{-1}) and analysing it in a quartz sample boat. Solid samples and standards were analysed in Ni boats. Reference materials GSJ JG-1a granodiorite (Geological Survey of Japan), LOAM soil (IRMM ERM-CC141, Institute for Reference Materials and Measurements, Belgium), and NIST SRM 2706 New Jersey soil (National Institute of Standards and Technology, USA) were analysed every one to six sample aliquots at the beginning to test the calibration set-up and then every ten to fifteen sample aliquots to routinely check the accuracy and precision within each and between all measurement sessions (see DMA-80 analytical workflow in online supporting information Table S2). During one of the runs, the Hg mass fraction of IAG MUH-1 (Ultramafic rock, Harzburgite, Kraubath) CRM (International

Association of Geoanalysts, Nottingham, UK) was measured for the first time. The DMA-80 cleaning procedure was performed before each analytical run, between each sample, and between reference materials and samples (Table S2) to ensure no carry-over in the instrument between samples: Ni sample boats were cleaned after runs by rinsing with high-purity water, soaking in nitric acid (HNO_3 1%) for 2 h, and then rinsing again with high-purity water before being dried at 700 °C for 2 h in a muffle furnace to desorb any remaining Hg. Three cleaned Ni sample boats were analysed during a measurement session to test the cleaning efficiency. The DMA-80 analyses were performed during seven measurement sessions (I to VII) between January 2023 and February 2024.

Sample acid digestion procedure

Sample acid digestion was performed only for AP powders due to the contamination issues in JAP and WCP powders (see Discussion) and the heterogenous grain sizes in AM powders. The acid-digested powders consist of two to four aliquots of AP powders of LS149 granite, VS134 diorite, Campore gabbro, and NZ2314A2 Balmuccia peridotite. However, an aliquot from AM powder from Campore gabbro was also acid-digested to test the efficiency of the procedure on the heterogeneous grain sizes. In addition, we acid-digested the leftover material after DMA-80 analyses from the AP powders for which DMA-80 gave the highest and lowest Hg values for the samples LS149 granite, Campore gabbro, and NZ2314A2 peridotite to assess the efficiency of DMA-80 in releasing all of Hg present in the sample. The same procedure was applied by Torres-Rodriguez et al. (2024) to verify that all Hg was released from combustion during AAS analyses. Note that it is common to refer to the residual powder after combustion as an ash product (e.g., Torres-Rodriguez et al. 2024). Nonetheless, we find it more appropriate to utilise the term "roasted" powders because the combustion process operated by the DMA-80 is similar to the material left after roasting cinnabar in a furnace, the process by which free Hg is obtained from its main mineral (Biester et al. 2000).

The powders were acid-digested in polytetrafluoroethylene (PTFE) vessels by total dissolution in a closed microwave system (Multiwave PRO, Anton Paar) at the Department of Chemical and Pharmaceutical Sciences, University of Trieste (Italy). For each sample, 0.250 to 0.256 g of powder was weighed, placed in the PTFE vessels, and Suprapure concentrated hydrochloric acid (HCl 37–39% v/v; VWR International) and nitric acid (HNO_3 67–69% v/v, VWR) were added in a 3:1 ratio, together with 6 ml of hydrofluoric acid (HF 47–51% v/v, VWR) (Loring and Rantala 1992, modified EPA Method 3052, USEPA 1996). After the first heating step in the microwave at 185 °C for 45 min and cooling at 50 °C for 22 min, boric acid (H_3BO_3, 6% v/v) was added to the solution to buffer the excess amount of HF. The PTFE vessels were then placed again in the microwave at 160 °C for 30 min and then cooled at 50 °C. Subsequently, all PTFE vessels were inspected for possible residual insoluble phases. In the PTFE vessels used to acid-digest LOAM soil and peridotite samples, dark, insoluble material (i.e., organic matter and spinels, respectively) was still present. No other unsoluble phases (e.g., zircons, oxides, etc.) were detected for the remaining samples. The solutions were transferred into metal-free vials and diluted to a volume of 25 ml by adding high-purity (Milli-Q) water and stored at 4 °C in a dark and protected space until analysis. Cleaning of PTFE vessels was performed every session of sample digestion with 2:1 HNO_3 and HCl and repeating heating step 1 in the microwave. Using the same analytical steps outlined above, during each chemical session, we also acid-digested JG-1a granodiorite and LOAM soil or NIST SRM 2706 New Jersey Soil RMs and prepared two blanks (i.e., acid solution without any sample or RM) for quality control and analytical performance, including checking for contamination. Before the main acid digestion sessions, we prepared different blanks ($n = 8$), again following the steps outlined above to inspect the Hg contribution of the acid used for the acid digestion procedure.

Cold vapour-atomic fluorescence spectroscopy (CV-AFS)

CV-AFS (Mercur, Analytic Jena) analyses were conducted at the Department of Mathematics, Informatics and Geoscience of the University of Trieste (Italy). Mercury mass fraction was determined after sample reduction with stannous chloride ($SnCl_2$; 2% in HCl 2% v/v; EPA Method 1631e, USEPA, 2002). Stannous chloride ($SnCl_2$) solution was prepared before each analysis and the quantity depended on the number of samples to be analysed. Between 2 and 8 g of stannous chloride dihydrate ($SnCl_2 \times 2H_2O$) was dissolved in 2 to 16 ml of concentrated HCl and let react for at least 40 min before diluting to the desired volume with high-purity water. For instance, 32 analyses require 8 g of $SnCl_2$ dissolved in 16 ml of HCl and diluted in 400 ml. The $SnCl_2$ solution was purged, along with the sample, during analyses with ultrapure Ar (99.9999%). Instrument calibration was performed for each measurement session using standard solutions (between 1 and 100 ng l^{-1}) prepared by diluting a Hg standard solution (NIST, 1 mg l^{-1}) and

acidifying with bromine chloride (BrCl, 500 µl/100 ml). The Hg determination was performed through a pre-reduction using hydroxylamine hydrochloride (NH_2OH-HCl) to buffer the excess of halogens produced during the addition of BrCl, followed by a reduction with $SnCl_2$ according to EPA Method 1631e (USEPA 2002). Analytical blanks and RMs (JG-1a and LOAM soil or NIST SRM 2706) were analysed in the same batch as the samples. Mercury was analysed in triplicate for each sample aliquot to investigate within-aliquot heterogeneity. In addition, for all but one sample (i.e., AM powder from Campore gabbro), Hg was analysed in two to four aliquots per sample to test within-sample heterogeneity. The Hg contribution from the acids, determined from the blank analyses, was subtracted from the results in ng l^{-1}, which were then corrected for the sample mass and dilution volume to ng g^{-1}. The CV-AFS analyses were performed during four measurement sessions (I through IV) between January 2023 and February 2024. Session I was devoted to blank analyses only.

Results

Individual measurement results from DMA-80 and CV-AFS analyses are shown in Tables S2 and S3, respectively. All uncertainties reported throughout the text are 2s.

Procedural blanks

DMA-80 cleaning procedures measurements ($n = 165$) run throughout the study had absorbance (i.e., Hg peak height) values for blanks (no boat or sample) between 0 and 0.051 A, with 9% of values between 0.002 and 0.051 A (Hg = 0.001–0.878 ng) and 91% ≤ 0.001 A (Hg ≤ 0.00001 ng (Figure 3a, b; see DMA-80 analytical workflow in Table S2). We observed that i) the highest absorbance values (≥ 0.002) were obtained at the beginning and rarely during the analytical runs and ii) the DMA-80 was clean (i.e., Hg < 1 pg) and ready for analysis of low Hg samples below an absorbance value of 0.001 A. The absorbance of the three analyses on empty, previously cleaned Ni sample boats (i.e., blanks) was between 0.004 and 0.022 A (Hg = 0.02–0.35 ng; Figure 3a, b).

Blanks ($n = 8$) during the first CV-AFS measurement session (Figure 4) resulted in a Hg concentration between 4.1 ± 0.1 and 7.3 ± 0.2 ng l^{-1} (mean = 5.4 ± 2.3 ng l^{-1}, RSD = 21%). Mercury from the blanks ($n = 2$) in the second run was 1.4 ± 0.01 ng l^{-1} (mean, RSD = 0.3%), whereas during the third ($n = 4$) and fourth ($n = 4$) runs, Hg contribution was similar to the first analyses, with mean of
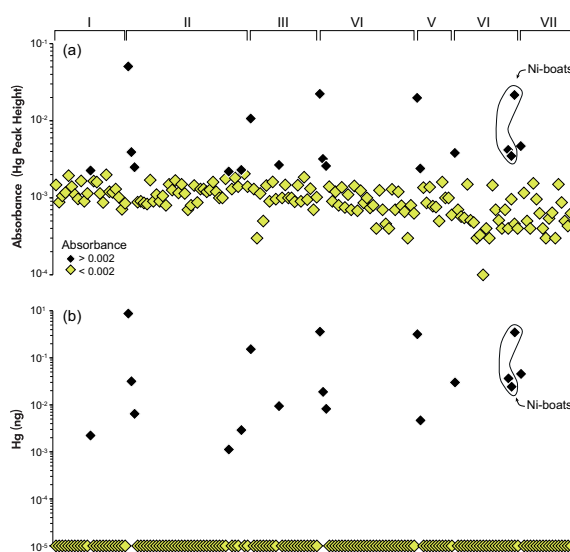

Figure 3. DMA-80 cleaning procedure. (a) Absorbance (Hg peak height) and (b) Hg contribution in ng for each cleaning step. Roman numerals indicate the measurement session.
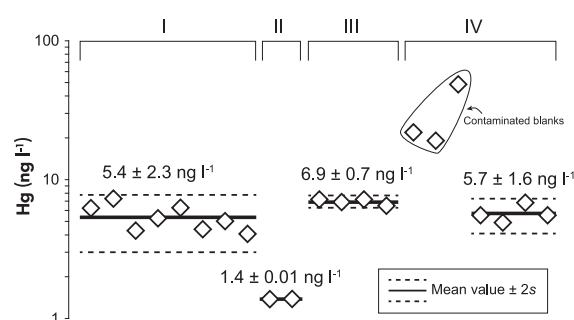

Figure 4. Procedural blanks analysed during CV-AFS analyses. 2s values are smaller than the symbols. Roman numerals indicate the measurement session.

6.9 ± 0.7 (RSD = 5%) and 5.7 ± 1.6 ng l^{-1} (RSD = 14%), respectively. Three blanks in session IV had Hg concentrations above 19 ng l^{-1}. These values were likely due to insufficient PTFE vessel cleaning and were excluded as outliers (Figure 4). The average value of the blanks (Figure 3) from each measurement session was subtracted from the Hg mass fractions obtained from the RMs and the samples in that session.

Validation through RMs

JG-1a contains a proposed value of 4.1 ng g^{-1} obtained from flame atomic absorption spectroscopy (FAAS,

Imai *et al.* 1995) or literature values of 3.5 ± 0.8 ng g⁻¹ from Nippon-Ash Model AA-855-AAS equipped with Model AMD mercury detector (CV-AAS, Terashima 1994), 4.1 ± 0.2 ng g⁻¹ from AMA-254 (CV-AAS, Hall and Pelchat 1997) and 4.1 ± 0.6 ng g⁻¹ from DMA-80 (Marie *et al.* 2014). Since the Hg value from Imai *et al.* (1995) is the proposed value according to GSJ, we planned to use this to calculate recovery for DMA-80 and CV-AFS. However, as no uncertainty was given, we therefore compiled the literature values (see Table 2) for FAAS and CV-AAS techniques from Imai *et al.* (1995, three sources in their appendix 1), Terashima (1994), and Hall and Pelchat (1997), noting that Terashima (1994) is one of the three sources included in Imai *et al.* (1995) so this was not counted twice. Thus, the calculated literature value we used for recovery was 4.1 ± 1.3 ng g⁻¹ (Table 2). Recovery values from individual DMA-80 analyses were between 73 and 137%, except for three analyses with Hg > 12 ng g⁻¹ (recovery > 300%; Figure 5, Table S2). When the three outliers are excluded, the mean is 3.8 ± 1.4 ng g⁻¹ (*n* = 37, RSD = 18%, recovery = 93%, Figure 5a), and all but one of the values are within 2*s* of the calculated literature value. For CV-AFS, measurement results were homogeneous within and between each measurement session (Figure 5b). Mercury results on JG-1a (*n* = 8) were similar to each other among the three measurement sessions with an overall mean value of 3.1 ± 0.4 ng g⁻¹ (overall RSD = 5.7%), and recoveries were between 66 and 80% (Figure 5, Table S3). The

Table 2.
Compilation of literature values and measurement results from this study to propose a new reference value for GSJ JG-1a granodiorite reference material

Source	Method[c]	Mean	2*s*	*n*
Imai *et al.* (1995), from Terashima (1994)	CV-AAS	3.5	0.8	
Imai *et al.* (1995), from Yamamoto (1990)	FAAS	3.72		
Imai *et al.* (1995), from Takenaka (1987)	FAAS	5		
Hall and Pelchat (1997)	CV-AAS	4.1	0.2	2
Calculated Literature Value[a]	*FAAS, CV-AAS*	*4.1*	*1.3*	*4*
This Study	CV-AFS	3.1	0.4	8
Proposed New Reference Value	***CV-AFS, FAAS, CV-AAS***	***3.9***	***1.5***	***5***
Marie *et al.* (2015)	DMA-80	4.1	0.6	2
This Study[b]	DMA-80	3.8	1.4	37

2*s* = two standard deviations.
n = the number of samples used in the calculation of mean and 2*s*.
[a] Calculated from the four literature values above it; used for calculating recovery in this study.
[b] Does not include three outliers (see text).
[c] CV = cold vapour; AAS = atomic absoption spectroscopy; F = flame; AFS = atomic fluorescence spectroscopy; DMA-80 = direct mercury analyser.

CV-AFS analyses of JG-1a were within 2*s* of the calculated literature value and were consistent with the lowest values observed by DMA-80.

Loam soil also has two certified reference values: 83 ± 17 ng g⁻¹ from total Hg analyses and 80 ± 8 ng g⁻¹ from aqua regia extractable content (IRMM certificate of analysis ERM- CC141, deVos *et al.* 2012). In this study, we used 83 ± 17 ng g⁻¹ for calculating recovery because it was obtained using the same sample acid digestion procedure (deVos *et al.* 2012) we adopted in this study. DMA-80 Hg analyses (*n* = 21) on the LOAM soil (Figure 5c) were accurate and precise, giving a mean of 81 ± 12 ng g⁻¹. Recovery values ranged from 86 to 113% (mean 97%). Mercury mass fractions from CV-AFS analyses (*n* = 7) during measurement sessions III and IV had an overall mean of 81 ± 10 ng g⁻¹; Figure 5d) with an RSD of 36% and recovery values between 91 and 105%. We observed a sudden drop toward lower Hg values between sessions III and IV, not explained by blank values, but still within 2*s* of the reference value.

The NIST SRM 2706 RM certificate provides a certified value of 132.9 ± 3.3 ng g⁻¹ (by CV-ID-ICP-MS) and a range obtained by EPA methods 7471 (CV-AAS) and 7473 (Direct Mercury Analyzer) of 120–140 ng g⁻¹ (*n* = 6, mean = 130, median = 120). We used the EPA mean and range since it includes the certified value and incorporates more than one analytical method. In this study, the DMA-80 analyses (*n* = 6) on NIST SRM 2706 were done only during sessions I and II and had an overall mean of 138 ± 7 ng g⁻¹ (RSD = 3%). Recoveries ranged from 102 to 110% (mean 106%, Figure 5e). Five out of six measurements were within the EPA range. A single CV-AFS analysis (session II) on this RM showed a value of 122 ng g⁻¹ with 94% recovery, which is within the EPA range (Figure 5f).

Mercury analyses on rock samples

The DMA-80 and CV-AFS analytical results of the powdered rock samples are presented in Figure 6. The DMA-80 analyses on all JAP powders showed high Hg values ranging from 20 to 61 ng g⁻¹ with within-batch (i.e., analyses of replicates from the same powder) RSD from 9 to 37%. DMA-80 analyses on replicates from WCP powders displayed variable within-batch heterogeneity with RSD from 3% in the granite to RSD of 116% in the Finero peridotite. Mercury mass fractions in WCP powders were below 10 ng g⁻¹ in the granite, diorite, and gabbro, between 13 and 19 ng g⁻¹ in the Balmuccia peridotite, and highly variable (from 2.8 to 31 ng g⁻¹) in Finero peridotite.
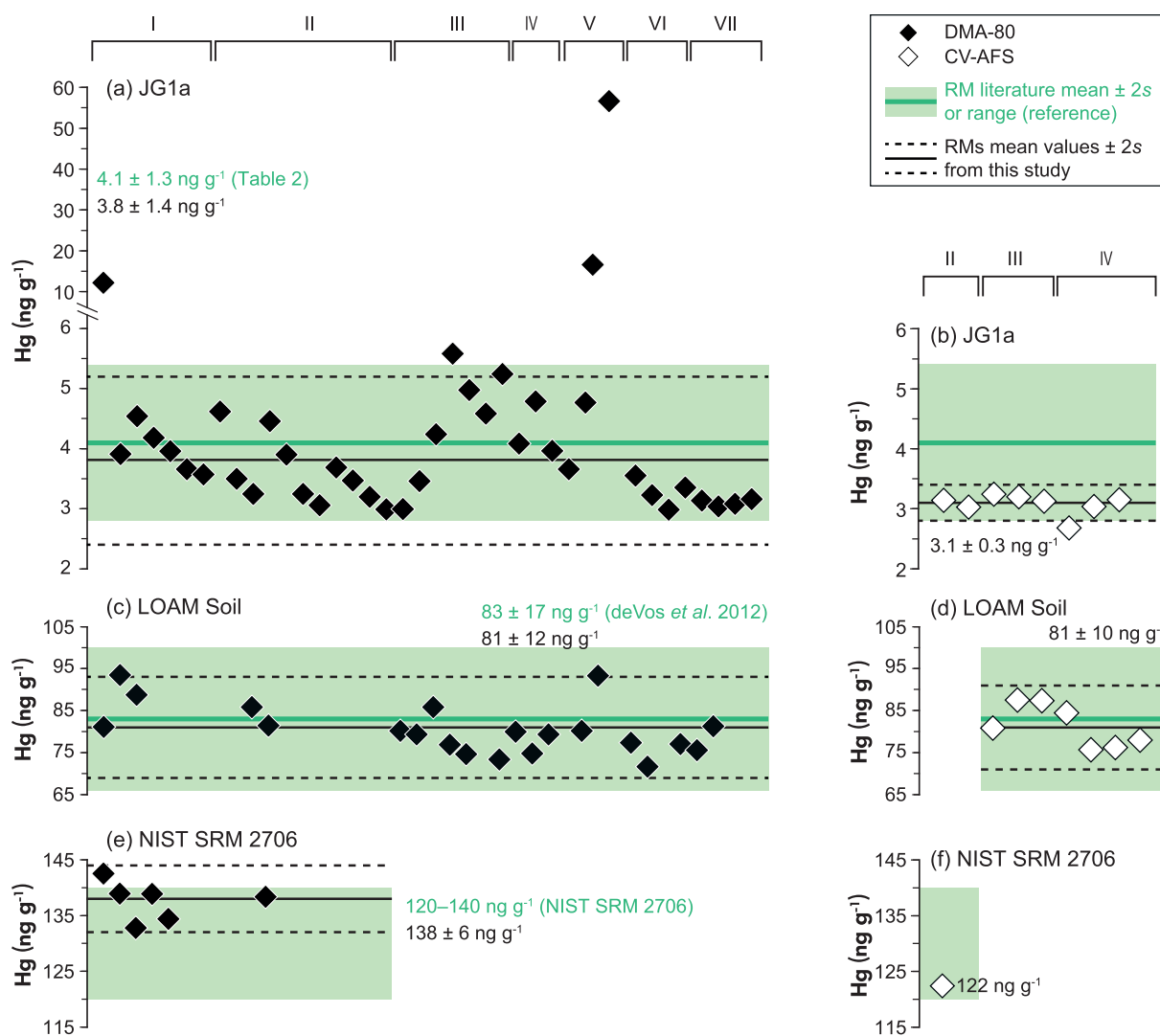
Figure 5. Mercury mass fraction (ng g^{-1}) in different reference materials during different measurement sessions. **(a, b) JG-1a** granodiorite, **(c, d) LOAM Soil** and **(e, f) NIST SRM 2706.** Black diamonds represent single DMA-80 analyses – hence, no standard deviation is indicated. Empty diamonds are CV-AFS measurements of aliquots analysed in triplicate. Reference material values in **(b), (d)** and **(f)** are those reported in **(a), (c),** and **(e),** respectively. Roman numerals indicate the measurement session. See text for more information.

Hand-made powders (AM) displayed variable within-batch heterogeneities with RSD from 12% in the orthogneiss to 62% in the Finero peridotite. In Balmuccia peridotite, Hg ranged from 11 to 14 ng g^{-1}, whereas all other samples exhibited Hg mass fractions from 1 to 10 ng g^{-1}. Similar observations could be traced for the AP powders. Except for the NZ2314A2 Balmuccia peridotite where the within-batch RSD was 7% as supported by the narrow Hg mass fractions (11 to 14 ng g^{-1}), the other samples displayed large within-batch heterogeneity confirmed by the RSD values ranging from 20% in the LS 149 granite (1.4 to 2.2 ng g^{-1}) to 87% in the gabbro (3.7 to 23.1 ng g^{-1}). The first DMA-80 analyses ($n = 5$) on the MHU-1 harzburgite CRM provided Hg mass

fractions between 8.7 and 9.5 ng g^{-1} and a mean of 9.2 ± 0.7 ng g^{-1} (RSD = 4%, Table S2).

Mercury analyses with CV-AFS on AP powders of LS149 granite still displayed high RSD (31%), yet mass fractions (mean of 1.56 ± 0.96 ng g^{-1}) were akin to those obtained by DMA-80 (Figure 6a). VS134 and Campore gabbro AP powders (Figure 6b, c) showed low within-batch variability (RSD < 11%) with Hg mass fractions (mean = 3.5 ± 0.6 [$n = 4$] and 3.4 ± 0.7 [$n = 2$] ng g^{-1}, respectively). These values were similar to the lowest values detected by DMA-80. This is further observed in the single analysis on a Campore gabbro AM powder (2.6 ng g^{-1}, Figure 6c). Conversely, CV-
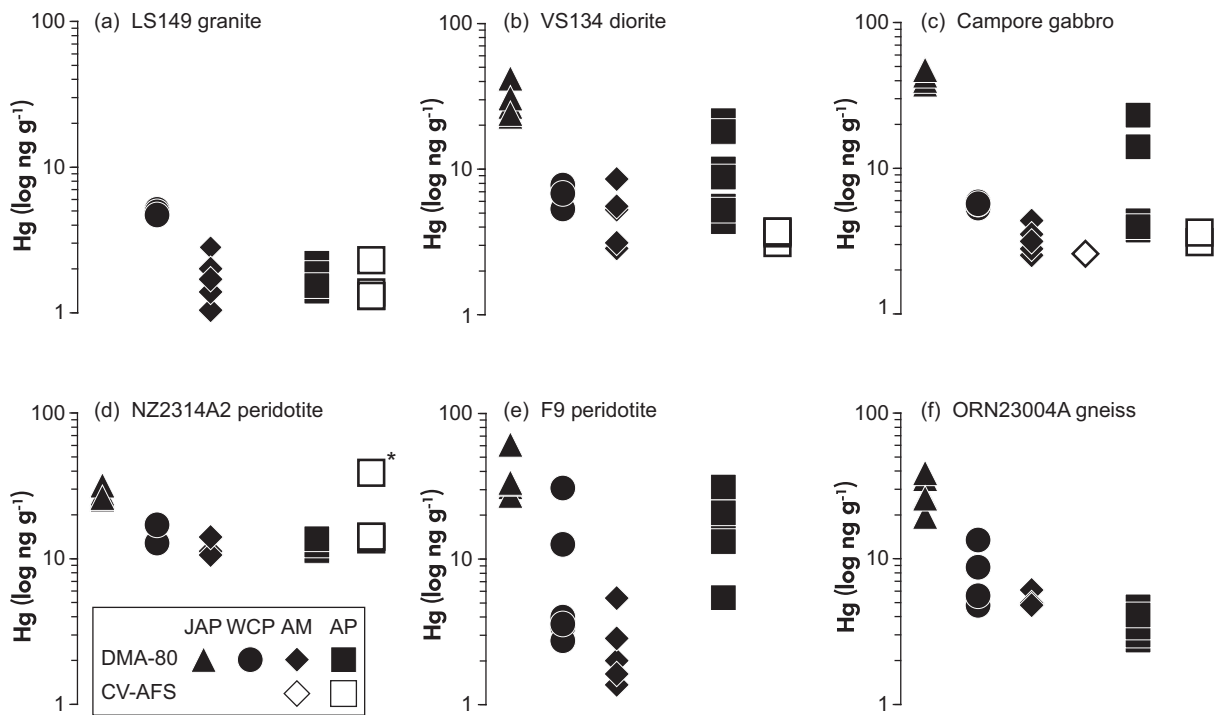
Figure 6. Plots of Hg mass fraction from analyses of rock samples by DMA-80 and CV-AFS. (a) LS149 granite, (b) VS134 diorite, (c) Campore gabbro, (d) NZ2314A2 Balmuccia peridotite, (e) F9 Finero peridotite, and (f) ORN23004A orthogneiss. WCP: tungsten carbide planetary mill; JAP: jaw crusher and agate planetary mill, AM: agate mortar and pestle; AP: agate planetary mill. Black diamonds represent single DMA-80 analyses – hence, no standard deviation is indicated. Open diamonds are CV-AFS measurements of aliquots analysed in triplicate. * Contaminated sample. See text for more information.

AFS analyses on NZ2314A2 peridotite AP powders had a mean Hg mass fraction of 14 ± 0.6 ng g^{-1}, similar to the highest value by DMA-80 and very low RSD, that is, 2%. As with the three blanks, a single aliquot with a high Hg mass fraction was discarded because it likely reflected contamination.

The CV-AFS analyses on DMA-80 roasted AP powders from LS149 granite, Campore gabbro, and NZ2314A2 peridotite (Figure 7a, b) showed different mass fractions. Peridotite powders have still more than 1 ng g^{-1} of Hg (1.5 ± 0.2, RSD 9%, $n = 2$), whereas in gabbro ($n = 2$) and granite ($n = 2$) roasted powders, 0.6 ± 0.3 ng g^{-1} (RSD 26%) and $< 0.1 \pm 0.2$ ng g^{-1} (RSD 82%) remained, respectively, the latter close to the detection limit of the instrument.

Discussion

Potential loss of mercury and cross-contamination

Frictional heating during sample powdering might lead to Hg volatilisation (e.g., Canil et al. 2015), but the temperature at which this occurs is unknown. Since the temperatures measured during milling were ≤ 40 °C, even after 1 h of AP powdering, no notable losses of Hg during our sample preparation were expected. This observation is supported by the experiments on Hg volatilisation performed by Coderre and Steinthorsson (1977). Their experiments consisted of heating at 1 atm, for 1 hour, and from 0 to 600 °C, two powders from two freshly crushed Icelandic basalts having ~ 4 and ~ 13 ng g^{-1} of Hg (acid digestion coupled with CV-AAS following Hatch and Ott 1968) and by measuring Hg mass fraction every 25, 50, or 100 °C. It was found that both samples had Hg mass fractions similar to the initial ones up to 50 °C (cf. Figure 1 in Coderre and Steinthorsson 1977). In contrast, Hg was lost above 50 °C, particularly from the powder with the highest Hg mass fractions. This powder lost 15% of its initial Hg content from 50 to 150 °C. Therefore, variabilities in Hg mass fractions observed in the present study within the same batch of powders and between samples are likely not related to Hg volatilisation. Canil et al. (2015) reached a similar conclusion by measuring similar Hg mass fractions on the samples powdered by hand and alumina ball mill. However, we

© 2025 The Author(s). *Geostandards and Geoanalytical Research* published by John Wiley & Sons Ltd on behalf of International Association of Geoanalysts.
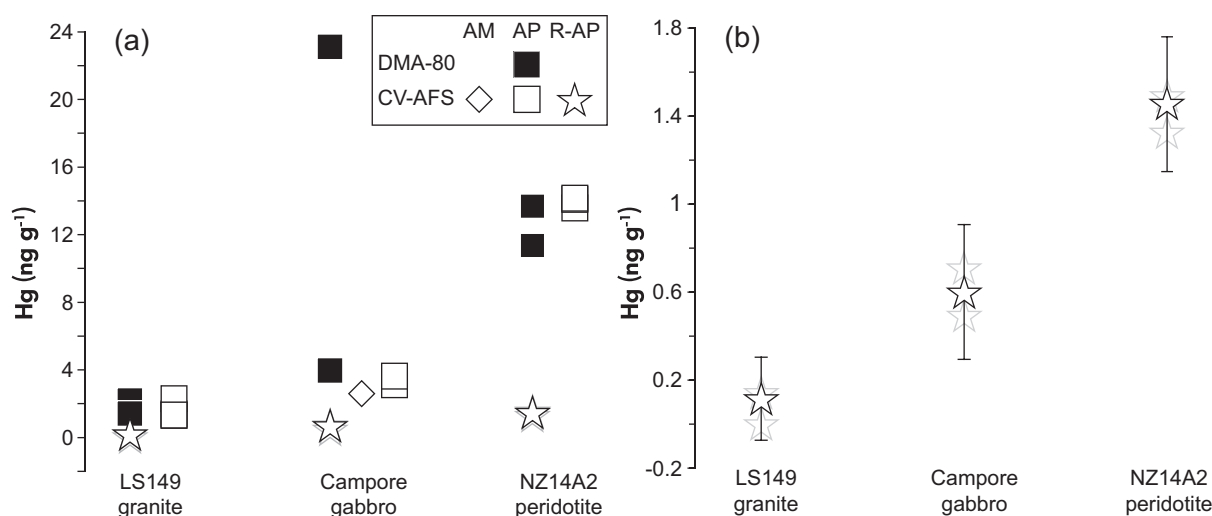
Figure 7. Testing the DMA-80 combustion efficiency. (a) Comparison between DMA-80 analyses, CV-AFS analyses on DMA-80 roasted powders (R-AP), and CV-AFS analyses. (b) Magnification on the CV-AFS analyses. AM: agate mortar and pestle; AP: agate planetary mill. In (a) and (b), bright stars represent the mean ± 2s from the two analyses on the DMA-80 roasted powders (faded stars). See the text for further explanation.

believe that this section of their Table 1 reports RSD rather than the stated "sd".

Mercury mass fractions of all JAP powders were, in general, higher (~ 20 ng g⁻¹) than those observed in AP and the other powders (Figure 6). Canil *et al.* (2015) also employed the jaw crusher before powdering, but they explained their extreme values as a nugget effect (see below). A general tendency towards high Hg mass fractions in WCP powders was also observed, although their variable RSD and Hg mass fractions are similar to AM and AP powders. The high within-batch variability in F9 Finero peridotite and ORN23004A2 could also be related to the inefficiency of WCP in milling all minerals (e.g., hydrated minerals) and to homogenise powders to small grain sizes (i.e., Figures S1b and S2b) which might lead to inefficient release of Hg from heterogeneous powders. Regardless of this last point, we suspect that the jaw crusher increased and homogenised Hg towards higher mass fractions, even after abundant cleaning and pre-conditioning, and the same conclusions can be drawn for WCP powders. Indeed, contamination from tungsten carbide mills is a common feature (Wang *et al.* 2013, Yamasaki 2018).

Sample mass and heterogeneity (i.e., nugget effect)

The Hg variability between the aliquots from the same batch of AM and AP powders and samples, as observed in

DMA-80 and between DMA-80 and CV-AFS analyses, was not related to Hg volatilisation or contamination during sample preparation. Canil *et al.* (2015) observed (Lumex RA-915+ analyses) large Hg variability, from 6 to 69 ng g⁻¹ (RSD 2 to 55%), in 5 mg powder samples and narrow Hg mass fractions (from 0.6 to 9 ng g⁻¹, RSD 2 to 36%) in 30 mg powders (Figure 2 in Canil *et al.* 2015). These authors suggest that the large Hg variability and highest RSD seen in small aliquots are related to the presence or absence of sulfides (i.e., nugget effect) in the various 5 mg aliquots of the same sample. They report that such an issue disappears in the 30 mg aliquots. However, when we include the results from Table 2, we see larger RSD in 30 mg (RSD 2 to 78%) than in 5 mg (RSD 2 to 40%) powders, which indicates that aliquot size was not the driving factor in this mass range.

In our study, we used large amounts of powder to obviate the nugget effect and aliquot size effects. Still, DMA-80 results showed a large range in Hg mass fractions from < 1 to 31 ng g⁻¹ with large RSD values from 7 to 87% in rock samples where AM and AP powder aliquots weighed between 250 and 256 mg (Figure 8a, b). For similar masses, the JG-1a granodiorite RM showed analogous Hg mass fractions (from 3 to 57 ng g⁻¹, Figure 9a) and even larger RSD (73 to 1389%), whereas LOAM soil RM displayed less variability in Hg content and RSD (from 72 to 93 ng g⁻¹ and from 4 to 11%, respectively). Intriguingly, the results obtained with CV-AFS on rock samples and JG-1a RM (Figures 8c and 9b, respectively) demonstrate that the
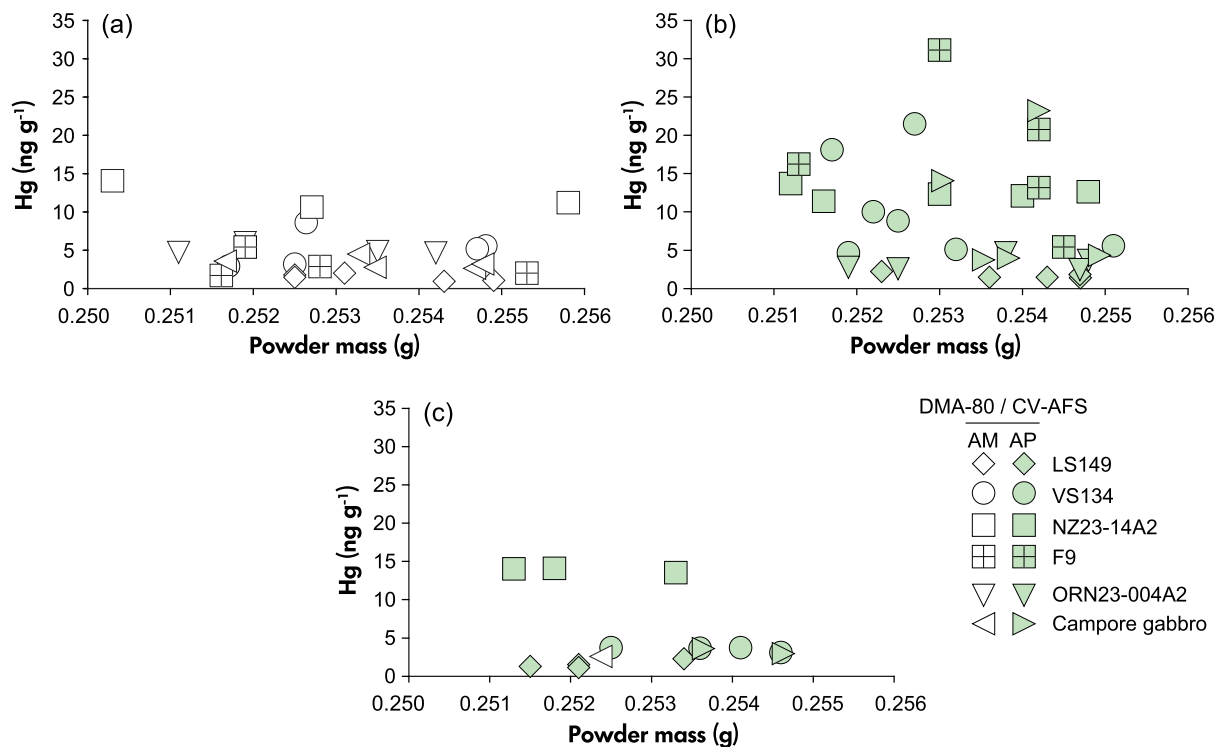
Figure 8. Plots of mercury mass fraction (ng g^{-1}) in samples against powder mass (g). In (a) and (b) DMA-80 analyses on AM and AP powders, respectively. (c) CV-AFS analyses on AP powders and a single AM powder.

Hg mass fractions of the aliquots of the powder analysed are similar. If sample heterogeneity were the cause of the highly variable DMA-80 results, we would expect to see some variation even in the aliquots of JG-1a RM and AP and AM rock powders analysed with CV-AFS. It is worth noting that all but one of the CV-AFS analyses on the AP powder replicates of LS149 granite are consistent and similar to the lowest value obtained through DMA-80 (Figure 6a). Analyses on this sample were performed during the fourth run session, where three blanks (Figure 4) and one NZ2314A2 replicate (Figure 6d) have extremely high values due to potential inefficient cleaning of the PTFE vessels. Note that all other results on NZ2314A2 peridotite aliquots (Figure 6d) are consistent with each other and the RMs analysed during this session are within the certified values (Figure 5b, d). Inefficient cleaning might explain the different LS149 granite aliquot, although the possibility of a small-scale sample inhomogeneity cannot be excluded. Sample inhomogeneity could be responsible for the increase in Hg mass fractions in LOAM soil RM seen during CV-AFS analyses within session III and the drop between sessions III and IV (Figure 5d). Similar variability is reported by deVos *et al.* (2012), and it can be ruled out that such Hg drop is from the Hg contribution of the blanks since CV-AFS analyses on the JG-1a RM in sessions III and IV are all consistent with each other.

In summary, we observed that powder mass did not affect the results of this work, and sample heterogeneity cannot be the cause for the variability of Hg mass fractions found among the different aliquots of powders in our samples and JG-1a RM. Nonetheless, at the present stage, we cannot exclude some minor nugget effects on a few of our analyses, even with large powder aliquots.

DMA-80 combustion efficiency

Mercury mass fractions analysed in the DMA-80 roasted AP powders by CV-AFS indicate any remaining Hg that was not released during the DMA-80 analysis. These results showed the lowest mass fractions for the LS149 granite (< 0.1 ± 0.2 ng g^{-1}) and the highest for the NZ2314A2 peridotite (1.5 ± 0.2 ng g^{-1}) (Figure 7b). The following observations can be made according to these results:

(i) The results of DMA-80 analyses on NZ2314A2 AP powders became consistent with those of CV-AFS analyses of AP powders (13.9 ± 0.6 ng g^{-1}) when the amount of Hg remaining after analyses with DMA-80 (1.5 ± 0.2 ng g^{-1}) was added to the DMA-80 result in the initial sample (12.5 ± 3.3 ng g^{-1}) (Figure 7). This indicates that a small amount
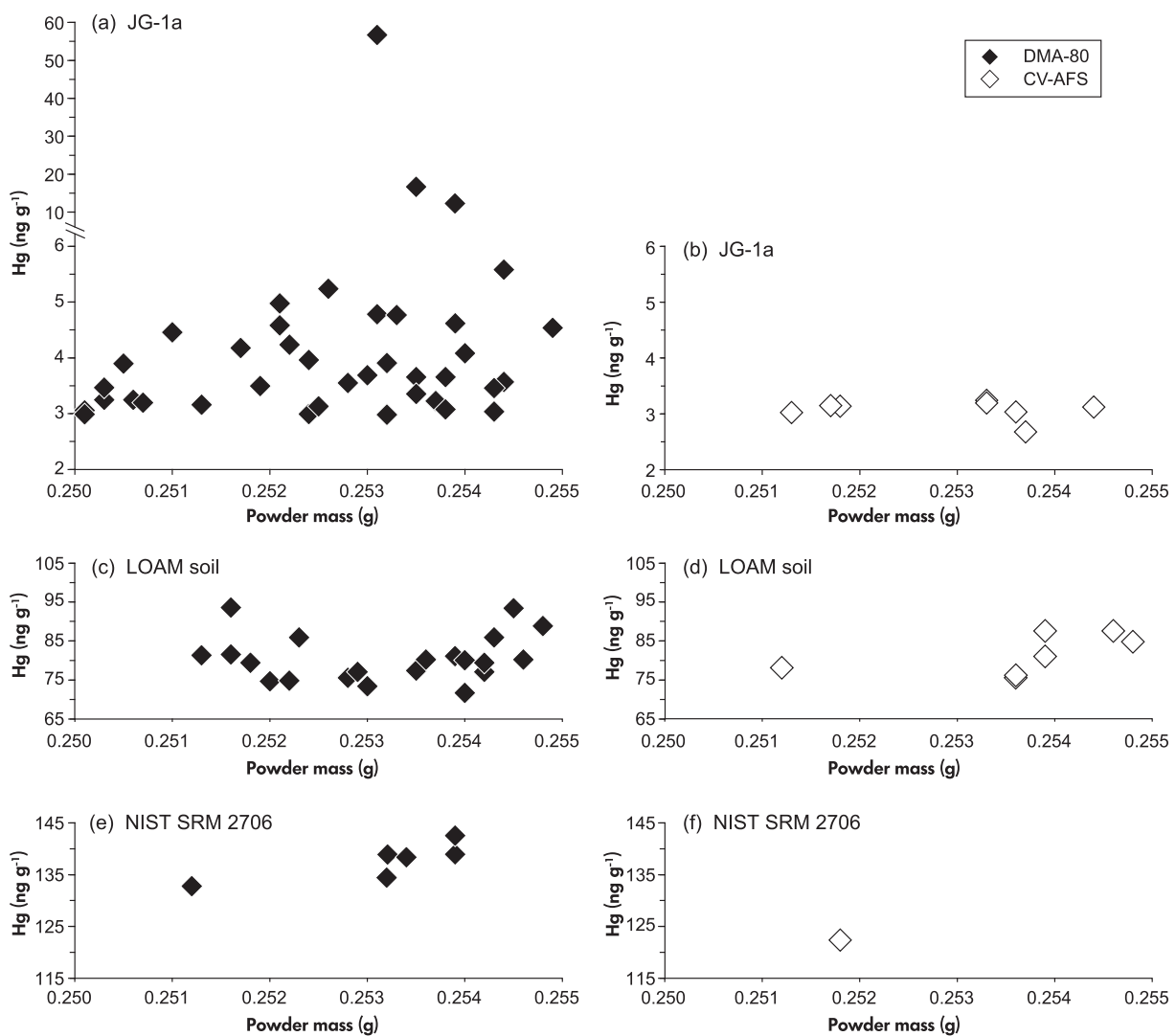
Figure 9. Mercury mass fraction (ng g^{-1}) in different reference materials plotted against the mass of powder (g).

of Hg is likely also hosted in olivine, pyroxenes, and spinels in addition to sulfides. Note that Lehloenya and Roelofse (2013), in their DMA-80 study on minerals of cumulates of Bushveld Complex (South Africa), describe that eight-folded Hg^{2+} could substitute eight-folded Ca^{2+} in the M2 site of augite since they have similar ionic radii (1.14 and 1.12 Å, respectively). Interestingly, Coderre and Steinthorsson (1977) found 9 and 5 ng g^{-1} of Hg in pyroxene phenocrysts and olivines separated from Jan Mayen ankaramite and Budahraun alkali olivine basalt, respectively. Alternatively, if all Hg is hosted in mantle-derived sulfides (e.g., Canil et al. 2015), DMA-80 may be incapable of releasing it from these minerals because of their high $T_{solidus}$ (> 1000 °C) at 1 atm (e.g., Zhang and Hirsmann 2016). In either case, DMA-80's operating conditions (combustion temperature of 650 °C, at 1 atm for 1.5 min) are inefficient in releasing all Hg from ultrabasic rocks (e.g., peridotites). Also, since spinels

can host chalcophile elements such as S, Cu, Se, Cd, In, and Pb (Bosi et al. 2019) and sulfide inclusions (Wang et al. 2013), we cannot exclude that the unsoluble spinels may retain Hg, hence biassing our CV-AFS analyses on NZ2314A2 peridotite AP powders.

(ii) The Hg results of CV-AFS analyses on Campore gabbro AP powders and on single AM powder are similar to one another and to the lowest values found after DMA-80 analyses for the same powders (Figure 6c), suggesting that this is the true value of this sample. However, if the small amount of the residual Hg in DMA-80 roasted powders is added to the results of DMA-80 analyses on the initial sample, the obtained mass fraction would not be comparable with that resulting from CV-AFS analyses (Figure 7a), simply because the DMA-80 result on the initial sample is already much higher than the CV-AFS result. The variations in

AM and AP powders seen for this sample (and VS134 diorite) are also related to other factors.

(iii) In the DMA-80 roasted LS149 AP powders, the Hg residue is extremely low, suggesting that combustion is more efficient in felsic rocks. However, it must be recalled that at 1 atm, the $T_{solidus}$ of granite is $\geq$ 900 °C (e.g., Stern et al. 1975). Therefore, as with peridotite and gabbro, it remains unknown how the DMA-80 instrument triggers the diffusion and/or release of Hg from rock-forming minerals.

The heterogeneous and large grain sizes observed within AM compared with AP powders (online supporting information Figures S1 and S2) could also bias the performance of DMA-80. In crystalline rocks, assuming that all Hg is hosted in the crystal lattice of the minerals (e.g., Jovanovic and Reed 1968), its release depends upon its diffusion kinetics, which is unknown, and the mineral sizes. For instance, if a sample powder or powder aliquots of the same sample are made of grains having heterogeneous sizes, the combustion of DMA-80 might be inefficient and provide inhomogeneous results since Hg will be preferentially released from smaller grains. Despite their different grain sizes, the DMA-80 Hg variations within and between AM and AP powders seem to contradict the above conclusions, as we would expect lower variation in finer-grained AP powders. It is possible that the effect exists but is blurred by another, larger, bias explained below. Therefore, we cannot exclude the possibility that grain size may also affect the capability of DMA-80 to release Hg from crystalline rocks.

Detection limits

It is important to stress that the highly variable Hg mass fractions we obtained over 1 year of analyses on the JG-1a RM (Figure 5a) suggest that DMA-80 experienced poor repeatability for samples with Hg $<$ 10 ng g^{-1}. The rather accurate and precise results on the LOAM soil and NIST-SRM 2706 (Hg $>$ 80 ng g^{-1}, Figure 5c–e) support this, and it is likely that Marie et al. (2014) did not observe any variation in their DMA-80 results as their sample batches and up to three replicates for each batch were analysed during a single day of analyses. When there were more than three replicates, they were analysed on different days (Marie et al. 2014), but this was mostly for environmental, soil, and sedimentary samples. Based on the results provided in this work, we conclude that DMA-80 provides spurious and imprecise analyses when rocks to be analysed have less than 10 ng g^{-1} of Hg mass fraction. That is, their mass

fraction is below the accuracy limit of the DMA-80 as defined by Marie et al. (2014). In this case, the DMA-80 is not precise relative to the range of Hg mass fractions that need to be investigated for crystalline rocks (0–20 ng g^{-1}). Marie et al. (2014) report a good correlation between their measurement results from different RMs and the recommended values for the same RMs above 20 ng g^{-1}. However, we also wonder whether their observations were biased because they investigated a large number of RMs together, consisting of environmental materials, sedimentary and crystalline rocks, and minerals, which all have different mass fractions and/or homogeneities.

The poor precision of the DMA-80 could also be responsible for the anomalous values observed in the blank Ni boats. Considering that our cleaning approach goes well beyond the manufacturer-recommended cleaning procedure, the blank values most likely represent artefacts of the DMA-80 due to its low reproducibility at low Hg mass fractions ($<$ 10 ng g^{-1}).

Conversely, the CV-AFS technique is more precise for all mass fractions with a very low limit of detection (1 pg g^{-1}; Bloom and Fitzgerald 1988, Pitcairn et al. 2006a, 2010, 2015, Hageman 2007, Butcher 2019) and, therefore, provides homogeneous and reproducible results. However, it remains unclear why DMA-80 and CV-AFS analyses on AP powders of LS149 granite (Figure 6a) are more consistent than in JG-1a RM (Figure 5a, b) despite the former having lower Hg mass fractions than the latter. A possible explanation is that both DMA-80 analyses on AM and AP powders of LS149 granite were performed during the seventh session (Figure 5a) when DMA-80 was not affected by poorer than usual precision. Additionally, based on the CV-AFS results from this study on NZ2314A2 Balmuccia peridotite and data from the study of Marie et al. (2014), we argue that DMA-80 precision might improve only above 30 ng g^{-1}. Therefore, based on our CV-AFS measurements, we report a mass fraction of 3.1 $\pm$ 0.4 ng g^{-1} Hg in JG-1a reference material (Table 2). We recommend that IAG MUH-1 be measured by a method such as CV-AFS since these DMA-80 results for this CRM were also $<$ 10 ng g^{-1}.

Implications

The low precision demonstrated for DMA-80 for Hg mass fractions below 20 ng g^{-1} raises doubts about the Hg data reported in the literature for crystalline rocks since ~ 50% of these were obtained using DMA-80 (Figure 1). Furthermore, as each point in Figure 1 is a single analysis or

the mean of two to five replicates, for which the standard deviation was rarely reported in the source dataset, *and* the accuracy and precision are based on the recovery percentages of the RMs (the results of which are rarely reported), it is unknown whether the values in Figure 1 reproduce the exact mass fraction in the investigated rock samples. In addition, when the results of this study are plotted together with those published in the literature (Figure 1), it can be seen that DMA-80 analyses on five replicates from AP powder of Campore gabbro and seven from AP powders of VS134 diorite and DMA-80 analyses from different basic/ultrabasic and intermediate rocks share similar Hg variabilities (Figure 1). This suggests that the large spread in Hg mass fractions observed between and among different rocks could be related to poor instrumental precision rather than simply representing actual variations in the Hg mass fractions, making the analyses less useful to constrain the geochemical processes.

Intriguingly, CV-AFS analyses on the Balmuccia peridotitic sample, which are devoid of contamination, are within the range of Hg mass fractions measured by Garuti *et al.* (1984) (Figure 1). Palme and O'Neil (2014) and Canil *et al.* (2015) suggest that the analyses presented by Garuti *et al.* (1984) suffered from contamination during sample manipulation. Nonetheless, the Balmuccia peridotitic body is sulfide-rich, and various studies (e.g., Wang *et al.* 2013, 2018, Wang and Becker 2015, 2018) have demonstrated that most of the chalcophiles and other highly incompatible elements record mantle metasomatism and interaction with late-stage crustal fluids. Hence, at least some Hg mass fractions observed by Garuti *et al.* (1984) are deemed reliable based on our results, although we cannot exclude that some high Hg mass fractions (> 100 ng g^{-1}) might be related to contamination (e.g., Canil *et al.* 2015).

It is worth recalling that Lumex RA-915+ instrumentation is similar to DMA-80, and therefore, it might be affected by the same instrumental biases seen for DMA-80. It also lacks the Au-amalgamator, which makes it even less precise and accurate than DMA-80, and its accuracy and precision in measuring Hg in crystalline rocks have never been carefully investigated. Consequently, the other ~ 32% of analyses and the Hg mass fraction of the primitive upper mantle proposed by Canil *et al.* (2015) (Figure 1), which is based on Lumex RA-915+ analyses on some Canadian Cordillera spinel mantle xenoliths, must be used with caution.

When we compile our CV-AFS results for JG-1a with literature values (Hall and Pelchat 1997, three sources from Imai *et al.* 1995 including Terashima 1994) for techniques with suitably low detection limits, we now have five independent sources using three analytical methods (CV-AAS, CV-AFS, and FAAS) and therefore propose a new reference value of 3.9 $\pm$ 1.5 ng g^{-1} Hg for GSJ JG-1a granodiorite (Table 2).

Conclusions

The results from this study demonstrate that DMA-80 is affected by different internal and external biases, such as sample heterogeneity, combustion inefficiency for some lithologies and grain sizes, and low reproducibility at low Hg mass fractions (< 10 ng g^{-1}). Therefore, this instrument is not precise in determining Hg mass fractions below 10 ng g^{-1} and possibly not even below 30 ng g^{-1}. Therefore, although based on an easy-to-use technique, DMA-80 is not recommended for measuring very low Hg mass fractions in crystalline rocks. Conversely, CV-AFS analyses are more precise despite being time-consuming. It should be noted that even CV-AFS results are not devoid of uncertainties, but scrupulous control of the acid digestion procedure can easily overcome this issue. From a compilation of our CV-AFS results and four literature sources using CV-AAS and FAAS methods, we propose a new Hg reference value of 3.9 $\pm$ 1.5 ng g^{-1} for GSJ JG-1a granodiorite reference material to replace the Imai *et al.* proposed value of 4.1 ng g^{-1} (Imai *et al.* 1995). Finally, because of the various uncertainties in measuring this element and the lack of care in reporting the analytical methods and data, we call for an international and standardised protocol for reporting Hg data to better track analytical accuracy, precision, and reproducibility.

Acknowledgements

Data availability statement

The data that support the findings of this study are available in the supplementary material of this article and online at https://doi.org/10.5281/zenodo.14577500.

References

Arevalo R. Jr. and McDonough W.F. (2010)
Chemical variations and regional diversity observed in MORB. Chemical Geology, 271, 70–85.

Bagnato E., Tamburello G., Avard G., Martinez-Cruz M., Enrico M., Fu X., Sprovieri M. and Sonke J.E. (2014)
Mercury fluxes from volcanic and geothermal sources: An update. In: Zellmer G.F., Edmonds M. and Straub S.M. (eds), The role of volatiles in the genesis, evolution and eruption of arc magmas. Geological Society, London Special Publication, 410, 263–285.

Biester H., Gosar M. and Covelli S. (2000)
Mercury speciation in sediments affected by dumped mining residues in the drainage area of the Idrija Mercury Mine, Slovenia. Environmental Science and Technology, 34, 3330–3336.

Bloom N. and Fitzgerald W.F. (1988)
Determination of volatile mercury species at the picogram level by low-temperature gas chromatography with cold-vapour atomic fluorescence detection. Analytica Chimica Acta, 208, 151–161.

Bosi F., Biagioni C., and Pasero M. (2019)
Nomenclature and classification of the spinel supergroup. European Journal of Mineralogy, 31, 183–192.

Butcher D.J. (2019)
Atomic fluorescence spectrometry. Encyclopedia of Analytical Science (3rd Edition), 1, 201–208.

Canil D., Crockford P.W., Rossin R. and Telmer K. (2015)
Mercury in some arc crustal rocks and mantle peridotites and relevance to the moderately volatile element budget of the Earth. Chemical Geology, 396, 134–142.

Coderre J.A. and Steinthorsson S. (1977)
Natural concentrations of mercury in Iceland. Geochimica et Cosmochimica Acta, 41, 419–424.

Coufalík P., Krmíček L, Zvěřina O., Meszarosová N., Hladil J. and Komárek J. (2018)
Model of mercury flux associated with volcanic activity. Bulletin of Environmental Contamination and Toxicology, 101, 549–555.

Coufalík P., Zvěřina O., Krmíček L, Pokorný R. and Komárek J. (2015)
Ultra-trace analysis of Hg in alkaline lavas and regolith from James Ross Island. Antarctic Science, 27, 281–290.

Covelli S., Faganeli J., Horvat M. and Brambati A. (2001)
Mercury contamination of coastal sediments as the result of long-term cinnabar mining activity (Gulf of Trieste, northern Adriatic Sea). Applied Geochemistry, 16, 541–558.

de Vos E., Engin E., Santoro A., Ricci M. and Held A. (2012)
The certification of the mass fraction of the total content and the aqua Regia extractable content of Hg in loam soil-ERM®-CC141. Publications Office of the European Union 2011, Scientific and Technical Research series, https://doi.org/10.2787/55675.

Deng C., Geng H., Xiao T., Chen D., Sun G. and Yin R. (2022a)
Mercury isotopic compositions of the Precambrian rocks and implications for tracing mercury cycling in Earth's interior. Precambrian Research, 373, 106646.

Deng C., Gou J., Sun D., Guangyi S., Tian Z., Lehmann B., Moynier F. and Yin R. (2022b)
Mercury isotopic composition of igneous rocks from an accretionary orogen: Implications for lithospheric recycling. Geology, 50, 1001–1006.

DMA-80 operating manual (2007)
Milestone.

Edmonds M., Mason E. and Hogg O. (2022)
Volcanic outgassing of volatile trace metals. Annual Review in Earth and Planetary Science, 50, 79–98.

Edwards B.A., Kushner S.S., Outridge P.M. and Wang F.Y. (2021)
Fifty years of volcanic mercury emission research: Knowledge gaps and future directions. Science of the Total Environment, 757, 143800.

Floreani F., Acquavita A., Petranich E. and Covelli S. (2019)
Diurnal fluxes of gaseous elemental mercury from the water-air interface in coastal environments of the northern Adriatic Sea. Science of the Total Environment, 668, 925–935.

Gao S., Luo T.C., Zhang B.R., Zhang H.F., Han Y.W., Hu Y.K. and Zhao Z.D. (1998)
Chemical composition of the continental crust as revealed by studies in east China. Geochimica et Cosmochimica Acta, 62, 1959–1975.

GEOSTANDARDS and GEOANALYTICAL RESEARCH

references

Garuti G., Gorgoni C. and Sighinolfi G.P. (1984)
Sulfide mineralogy and chalcophile and siderophile element abundances in the Ivrea-Verbano mantle peridotites (western Italian Alps). Earth and Planetary Science Letters, 70, 69–87.

Gworek B., Dmuchowski W. and Baczewska-Dąbrowska A.H. (2020)
Mercury in the terrestrial environment: A review. Environmental Science Europe, 32, 128.

Hageman P.L. (2007)
Determination of mercury in aqueous and geologic materials by continuous flow–cold vapor–atomic fluorescence spectrometry (CVAFS). U.S. Department of the Interior, USGS, Techniques and Methods, 5, D2.

Hall G.E.M and Pelchat P. (1997)
Evaluation of a direct solid sampling atomic absorption spectometer for the trace element determination of mercury in geological samples. The Analyst, 122, 911–924.

Hammerli J., Spandler C. and Oliver N.H.S. (2016)
Element redistribution and mobility during upper crustal metamorphism of metasedimentary rocks: An example from the eastern Mount Lofty Ranges, South Australia. Contributions to Mineralogy and Petrology, 171, 1–21.

Hatch WR., and Ott W.L. (1968)
Determination of sub-microgram quantities of mercury by atomic absorption spectrophotometry. Analytical Chemistry Journal, 40, 2085–2087.

Imai N., Terashima S., Itoh S. and Ando A. (1995)
1994 compilation of analytical data for minor and trace elements in seventeen GSJ geochemical reference samples "Igneous Rocks Series". Geostandards Newsletter, 19, 135–213.

Jovanovic S. and Reed G.W. (1968)
Hg in metamorphic rocks. Geochimica et Cosmochimica Acta, 32, 341–346.

Karakas O., Wotzlaw J.F., Guillong M., Ulmer P., Brack P., Economos R., Bergantz G.W., Sinigoi S. and Bachmann O. (2019)
The pace of crustal-scale magma accretion and differentiation beneath silicic caldera volcanoes. Geology, 47, 719–723.

Kushner D.S., Lopez T.M., Wallace K.L., Damby D.E., Kern C. and Cameron C.E. (2023)
Estimates of volcanic mercury emissions from Redoubt Volcano, Augustine Volcano, and Mount Spurr eruption ash. Frontiers in Earth Science, 11, 1–12.

Lehloenya P.B. and Roelofse F. (2013)
Mercury distribution amongst co-existing silicates within the Bushveld Complex. Chemie der Erde (Geochemistry), 73, 261–266.

Loring H.D. and Rantala R. (1992)
Manual for the geochemical analyses of marine sediments and suspended particulate matter. Earth-Science Reviews, 32, 235–283.

Marie B., Marin L., Martin P.Y., Gulon T., Carignan J. and Cloquet C. (2014)
Determination of mercury in one hundred and sixteen geological and environmental reference materials using a direct mercury analyser. Geostandards and Geoanalytical Research, 39, 71–86.

McDonough W.F. and Sun S. (1995)
The composition of the Earth. Chemical Geology, 120, 223–253.

Melendez-Perez J.J. and Fostier A.H. (2013)
Assessment of Direct Mercury Analyzer® to quantify mercury in soils and leaf samples. Journal of Brazilian Chemical Society, 24, 1880–1886.

Palme H. and O'Neill H.St.C. (2014)
Cosmochemical estimates of mantle composition. In: Holland H.D. and Turekian K.K. (eds), Treatise on geochemistry (2nd edition). Elsevier (Oxford), 3.1, 1–39.

Peters E. (1976)
Direct leaching of sulfides: Chemistry and applications. Metallurgical Transactions, B 7B, 505–517.

Pirrone N., Cinnirella S., Feng X., Finkelman R.B., Friedli H.R., Leaner J., Mason R., Mukherjee A.B., Stracher G.B., Streets D.G. and Telmer K. (2010)
Global mercury emissions to the atmosphere from anthropogenic and natural sources. Atmospheric Chemistry and Physics, 10, 5951–5964.

Pistone M., Ziberna L., Hetényi G., Scarponi M., Zanetti A. and Müntener O. (2020)
Joint geophysical-petrological modeling on the Ivrea geophysical body beneath Valsesia, Italy: Constraints on the continental lower crust. Geochemistry, Geophysics, Geosystems, 21, e2020GC009397.

Pitcairn I.K., Craw D. and Teagle D.A.H (2014)
The gold conveyor belt: Large scale gold mobility in an active orogen. Ore Geology Reviews, 62, 129–142.

Pitcairn I.K., Craw D. and Teagle D.A.H. (2015)
Metabasalts as sources of metals in orogenic gold deposits. Mineralium Deposita, 50, 373–390.

Pitcairn I.K., Olivo G.R., Teagle D.A.H. and Craw D. (2010)
Sulfide evolution during prograde metamorphism of the Otago and Alpine Schists, New Zealand. The Canadian Mineralogist, 48, 1267–1296.

Pitcairn I.K., Teagle D.A.H., Craw D., Olivo G.R., Kerrich R., Brewer T.S. (2006a)
Sources of metals in orogenic gold deposits: Insights from the Otago and Alpine Schists, New Zealand. Economic Geology, 101, 1525–1546.

Pitcairn I.K., Warwick P.E., Milton J.A. and Teagle D.A.H. (2006b)
A method for ultra-low level analysis of gold in rocks. Analytical Chemistry, 78, 1280–1285.

Rudnick R.L. and Gao S. (2014)
Composition of the continental crust. In: Rudnick R.L. (ed.), Treatise on geochemistry, 4. Elsevier (New York), 1–51.

GEOSTANDARDS and GEOANALYTICAL RESEARCH

references

Salters V.J.M. and Stracke A. (2004)
Composition of the depleted mantle. Geochemistry, Geophysics, Geosystems, 5, Q05B07, https://doi.org/10.1029/2003GC000597.

Sholupov S., Pogarev S., Ryzhov V., Mashyanov N. and Stroganov A. (2004)
Zeeman atomic absorption spectrometer RA-915+ for direct determination of mercury in air and complex matrix samples. Fuel Processing Technology, 85, 473–485.

Sinigoi S., Quick J. E., Demarchi G. and Klötzli U.S. (2016)
Production of hybrid granitic magma at the advancing front of basaltic underplating: Inferences from the Sesia Magmatic System (south-western Alps, Italy). Lithos 252–253, 109–122.

Smith C.N., Kesler S.E., Blum J.D. and Rytuba J.J. (2008)
Isotope geochemistry of mercury in source rocks, mineral deposits and spring deposits of the California Coast Ranges, USA. Earth Planetary Science Letters, 269, 399–407.

Stern C.R., Huang W.L. and Wyllie P.J. (1975)
Basalt-andesite-rhyolite-H_2O: Crystallisation intervals with excess H_2O and H_2O-undersaturated liquidus surfaces to 35 kilobars. Earth Planetary Science Letters, 28, 189–196.

Tavazzani L, Peres S., Sinigoi S., Demarchi G. and Musumeci G. (2017)
Structure and petrography of the Valle Mosso pluton, Sesia magmatic system, Southern Alps. Journal of Maps, 13, 684–697.

Tavazzani L, Peres S., Sinigoi S., Demarchi G., Economos R. C. and Quick J.E. (2020)
Timescales and mechanisms of crystal-mush rejuvenation and melt extraction recorded in Permian plutonic and volcanic rocks of the Sesia magmatic system (southern Alps, Italy). Journal of Petrology, 61, egaa049.

Tavazzani L, Wotzlaw J.-F., Economos R., Sinigoi S., Demarchi G., Szymanowski D., Laurent O., Bachmann O. and Chelle-Michou C. (2023)
High-precision zircon age spectra record the dynamics and evolution of large open-system silicic magma reservoirs. Earth and Planetary Science Letters, 623, 118432.

Terashima S. (1994)
Determination of mercury in one hundred and eighteen geochemical reference samples by cold vapor atomic absorption spectrometry. Geostandards Newsletter, 18, 199–202.

Tian Z., Lehmann B., Deng C., Luo A., Zhang X., Moynier F. and Yin R. (2023)
Mercury abundance and isotopic composition in granitic rocks: Implications for Hg cycling in the upper continental crust. Geochimica et Cosmochimica Acta, 361, 200–209.

Torres-Rodriguez N., Yuan J., Petersen S., Dufour A., González-Santana D., Chavagnac V., Planquette H., Horvat M., Amouroux D., Cathalot C., Pelleter E., Sun R., Sonke J.E., Luther G.W. and Heimbürger-Boavida L.E. (2024)
Mercury fluxes from hydrothermal venting at mid-ocean ridges constrained by measurements. Nature Geoscience, 17, 51–57.

U.S. EPA (1996)
Method 3052 – Microwave assisted acid digestion of siliceous and organically based matrices. Test methods for evaluating solid waste. U.S. Environmental Protection Agency (Washington, D.C., USA).

U.S. EPA (2002)
Method 1631, Revision E: Mercury in water by oxidation, purge and trap, and cold vapor atomic fluorescence spectrometry. U.S. Environmental Protection Agency (Washington, D.C., USA).

U.S. EPA (2007)
Method 7473 Report – Mercury in solids and solutions by thermal decomposition, amalgamation and atomic absorption spectrophotometry. U.S. Environmental Protection Agency (Washington, D.C., USA).

Ulmer P. (2000)
Partial melting in the mantle wedge – The role of H_2O in the genesis of mantle-derived 'arc-related' magmas. Physics of the Earth and Planetary Interiors, 127, 215–232.

Wang X., Deng C., Yang Z., Zhu J.J. and Yin R. (2021)
Oceanic mercury recycled into the mantle: Evidence from positive Δ^{199}Hg in lamprophyres. Chemical Geology, 584, 120505.

Wang Z. and Becker H. (2015)
Abundances of Ag and Cu in mantle peridotites and the implications for the behavior of chalcophile elements in the mantle. Geochimica et Cosmochimica Acta, 160, 209–226.

Wang Z. and Becker H. (2018)
Molybdenum partitioning behavior and content in the depleted mantle: Insights from Balmuccia and Baldissero mante tectonites (Ivrea Zone, Italian Alps). Chemical Geology, 499, 138-150.

Wang Z., Becker H. and Gawronski T. (2013)
Partial re-equilibration of highly siderophile elements and the chalcogens in the mantle: A case study on the Baldissero and Balmuccia peridotite massifs (Ivrea Zone, Italian Alps). Geochimica et Cosmochimica Acta, 108, 21–44.

Wang Z., Lazarov M., Steinmann L.K., Becker H., Zou Z. and Geng X. (2018)
The distribution of lead and thallium in mantle rocks: Insights from the Balmuccia peridotite massif (Italian Alps). American Mineralogist, 103, 1185–1199.

Yamasaki T. (2018)
Contamination from mortars and mills during laboratory crushing and pulverizing. Bulletin of the Geological Survey of Japan, 69, 201–210.

references

Yin R., Chen D., Pan X., Deng C., Chen L., Song X., Yu S., Zhu C., Wei X., Xu Y., Feng X., Blu J.D. and Lehmann B. (2022)
Mantle Hg isotopic heterogeneity and evidence of oceanic Hg recycling into the mantle. **Nature Communications, 13,** 1–7.

Zhang Z. and Hirschmann M.M. (2016)
Experimental constraints on mantle sulfide melting up to 8 GPa. **American Mineralogist, 101,** 181–192.

Zintwana M.P., Cawthorn R.G., Ashwal L.D., Roelofse F. and Cronwright H. (2012)
Mercury in the Bushveld Complex, South Africa, and the Skaergaard Intrusion, Greenland. **Chemical Geology, 320,** 147–15.

Supporting information

The following supporting information may be found in the online version of this article:

Figure S1. Grain-size images of powders from the Campore gabbro prepared for Hg determinations.

Figure S2. Grain-size images of powders from the NZ2414A2 Balmuccia peridotite prepared for Hg determinations.

Table S1. Data set of measurement results for mercury.

Table S2. DMA-80 measurement results.

Table S3. CV-AFS measurement results.

This material is available from: http://onlinelibrary.wiley.com/doi/10.1111/ggr.12606/abstract (This link will take you to the article abstract).